Splitting of antiferromagnetic resonance modes in the quasi-two-dimensional collinear antiferromagnet $Cu(en)(H_2O)_2SO_4$

V. N. Glazkov,[1,2,*] Yu. V. Krasnikova,[1,2] I. K. Rodygina,[1,3] J. Chovan,[4,5] R. Tarasenko,[6] and A. Orendáčová[6]

[1]*P.L. Kapitza Institute for Physical Problems, RAS, Kosygina 2, Moscow 119334, Russia*

[2]*International Laboratory for Condensed Matter Physics, National Research University "Higher School of Economics," Myasnitskaya strasse 20, 101000 Moscow, Russia*

[3]*Faculty of Physics, National Research University "Higher School of Economics," Myasnitskaya strasse 20, 101000 Moscow, Russia*

[4]*IT4Innovations National Supercomputing Center, VSB-Technical University of Ostrava, 17, listopadu 2172/15, CZ 708 33 Ostrava, Czech Republic*

[5]*International Clinical Research Center, St. Anne's University Hospital, Pekarska 53, 656 91 Brno, Czech Republic*

[6]*Institute of Physics, P. J. Šafárik University, Park Angelinum 9, 040 00 Košice, Slovakia*

(Received 26 July 2019; revised manuscript received 27 November 2019; published 10 January 2020)

A low-temperature magnetic resonance study of the quasi-two-dimensional antiferromagnet $Cu(en)(H_2O)_2SO_4$ ($en = C_2H_8N_2$) was performed down to 0.45 K. This compound orders antiferromagnetically at 0.9 K. The analysis of the resonance data within the hydrodynamic approach allowed us to identify anisotropy axes and to estimate the anisotropy parameters for the antiferromagnetic phase. Dipolar spin-spin coupling turns out to be the main contribution to the anisotropy of the antiferromagnetic phase. The splitting of the resonance modes and its nonmonotonous dependence on the applied frequency were observed below 0.6 K in all three field orientations. Several models are discussed to explain the origin of the nontrivial splitting, and the existence of inequivalent magnetic subsystems in $Cu(en)(H_2O)_2SO_4$ is chosen as the most probable source.

DOI: 10.1103/PhysRevB.101.014414

I. INTRODUCTION

Low-dimensional antiferromagnets are one of the focus topics of modern magnetism. Low dimensionality of the spin system enhances the role of thermal and quantum fluctuations, retarding magnetic ordering in these systems to the lower temperatures $T_N \ll \Theta$ (here Θ is a Curie-Weiss temperature) or even fully suppressing it. This yields the extended temperature range of the spin-liquid behavior where short-range spin-spin correlations determine the dynamics of the disordered spin system. "Freezing" of this spin liquid under the effect of weak coupling between the low-dimensional subsystems, additional further-neighbor or anisotropic interactions, external field, or applied pressure is of interest since the competing weaker interactions sometimes give rise to complex magnetic phase diagrams or to the appearance of the unusual (e.g., spin-nematic) phases [1–5].

Two-dimensional (2D) antiferromagnets are also of interest due to the occurrence of topological excitations induced by the magnetic field and/or the easy-plane spin anisotropy [6,7]. A crossover between the low- and high-temperature regimes of the spin dynamics appears in the vicinity of the topological Berezinskii-Kosterlitz-Thouless (BKT) transition accompanied by the formation of the bound pairs of vortex-antivortex excitations [8].

The recently studied antiferromagnet $Cu(en)(H_2O)_2SO_4$ [here $(en) = C_2H_8N_2$] is an example quasi-2D system. The combination of the thermodynamic measurements [9,10] and first-principles calculations [11] proved that its spin subsystem can be envisioned as a three-dimensional (3D) array of coupled zigzag square lattices with the strongest in-plane exchange coupling constant $J/k_B \simeq 3.5$ K and the interplane coupling $J' < 0.03J$ [9]. $Cu(en)(H_2O)_2SO_4$ orders antiferromagnetically at $T_N = (0.91 \pm 0.02)$ K; the ordering is accompanied by a sharp λ-like anomaly in the specific heat and by the appearance of the strong anisotropy in the magnetic susceptibility. The $(H - T)$ phase diagram was discussed in the context of a field-induced BKT transition [9,12]. Observed enhancement of the field-induced transition temperatures qualitatively follows predictions for the field-induced BKT transition [6]; this feature is characteristic of quasi-2D antiferromagnets [13].

In this paper we report the results of the low-temperature electron spin resonance study of the magnetic ordering in $Cu(en)(H_2O)_2SO_4$ down to 0.45 K. Magnetic resonance spectroscopy of the ordered phase probes the $q = 0$ magnon spectrum with high energy resolution (a routine resolution of 1 GHz corresponds to 0.005 meV), thus giving insight into the structure of the magnetic phase, type of magnetic ordering, magnetic phase transitions, etc. Our observations confirmed collinear ordering in $Cu(en)(H_2O)_2SO_4$ and allowed us to unambiguously identify the anisotropy axes and to determine the anisotropy parameters of the ordered phase. Observed anisotropy can be successfully described by dipole-dipole interaction. We also observed splitting of the resonance lines in the ordered phase, indicating the presence of inequivalent antiferromagnetic subsystems below the Néel temperature.

*glazkov@kapitza.ras.ru

II. EXPERIMENTAL DETAILS, SAMPLES, AND CRYSTAL STRUCTURE

Electron spin resonance (ESR) experiments were performed using a set of homemade transmission-type spectrometers covering a frequency range from 4 to 120 GHz; some of the spectrometers were equipped with ^{3}He-vapor pumping cryostats, allowing us to reach a temperature as low as 0.45 K. Magnetic fields up to 12 T were created by compact superconducting cryomagnets. Resonance absorption was recorded as dependence of the transmitted microwave power on the slowly swept magnetic field.

For most of our experiments samples were mounted on the bottom of the cylindrical (above 20 GHz) or rectangular (9–20 GHz) multimode microwave cavity. A small sapphire block was used as a heat link for the sample orientations, preventing plane-on-plane sample mounting. Low-frequency ESR experiments at frequencies of 4–8 GHz were performed in $\mathbf{H}||b$ orientation only with the help of a quasitoroidal resonator.

$Cu(en)(H_2O)_2SO_4$ (CUEN) crystals were grown by the same technique as the samples used in Ref. [9]. $Cu(en)(H_2O)_2SO_4$ crystallizes in the base-centered monoclinic space group C^6_{2h}. The (bc) planes are stacked in the $(1/2, 1/2, 0)$ direction. The primitive unit cell contains two copper ions; positions of these ions are linked by inversion. The second-order rotational axis is parallel to the b axis and passes through the copper ions. A fragment of the crystal structure of CUEN is shown in Fig. 1. As-grown crystals of $Cu(en)(H_2O)_2SO_4$ are blue-colored elongated thin plates with the long edge parallel to the a direction and the sample plane normal to the b direction. Sample shape allowed easy positioning of the sample at $\mathbf{H}||a, b, c^*$.

The formation of 2D planes of exchange-coupled spins was confirmed by the characteristic behavior of the specific heat and magnetization and by first-principles calculations [9–11]. Relevant exchange bonds are shown in Fig. 1. The in-plane coupling values are (in the notations of Fig. 1 and Ref. [11]) $J_4 = 3.4$–3.7 K and $J_6 = 0.35J_4$ [9]. Inversion centers in the middle of in-plane copper-copper bonds forbid the in-plane Dzyaloshinskii-Moriya (DM) interaction. However, the interplane DM coupling is possible along the J_1 and J_2 bonds [9,14]. The same inversion symmetry ensures the same orientation of g-tensor axes for two copper ions within the primitive unit cell.

III. EXPERIMENTAL RESULTS

Above the Néel point we observed a single-component paramagnetic resonance line with the g factor values determined from 10–120-GHz measurements as $g_a = 2.28 \pm 0.02$, $g_b = 2.06 \pm 0.02$, and $g_{c^*} = 2.07 \pm 0.02$. The g factor values found are in agreement with the earlier results [10,14]. No splitting of the ESR line was observed at $T > T_N$ both in all principal field orientations and in the control experiment with rotation of the applied field in the (ac^*) plane performed at the microwave frequency of 72.7 GHz (with the resonance fields around 24 kOe).

The antiferromagnetic transition point is marked by the shift of the resonance absorption from the paramagnetic

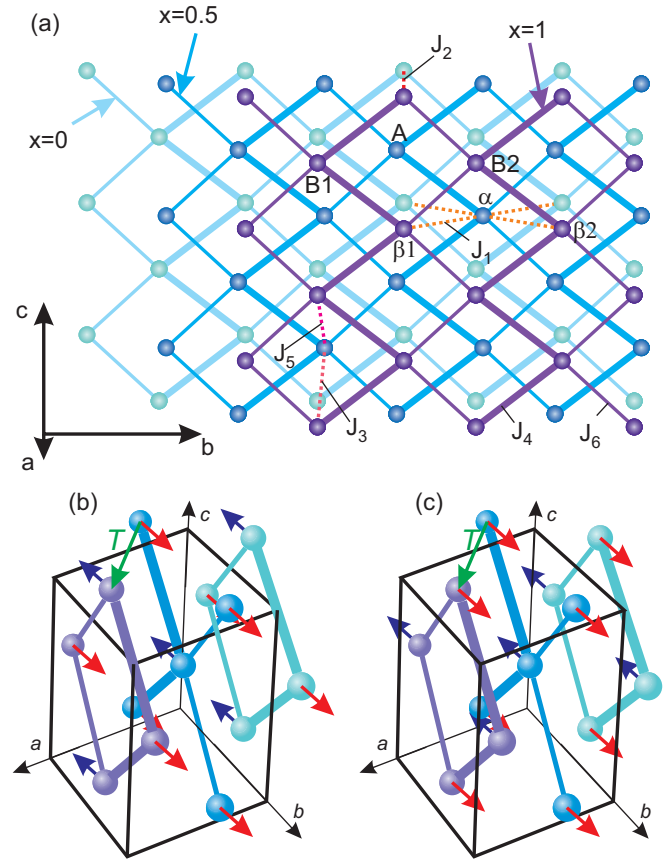

FIG. 1. (a) Fragment of the $Cu(en)(H_2O)_2SO_4$ crystal structure projected on the (bc) plane. Only copper ions are shown; thicker lines correspond to the strongest in-plane couplings. Layers shown by different shades of color are formed by atoms with a fractional x coordinate of 0, 0.5, and 1.0. Relevant in-plane and interplane couplings are shown according to Ref. [11]. Ions within the adjacent (ab) planes coupled by the DM interaction are marked as A, B1, and B2 (α, $\beta 1$, and $\beta 2$). Schemes of (b) antiferromagnetic and (c) ferromagnetic stacking of the antiferromagnetically ordered (bc) planes; blue and red arrows show ordered magnetic moment orientation, and green arrows show elementary translation $\mathbf{T} = (\mathbf{a} + \mathbf{b})/2$ linking the neighboring planes.

position (see Fig. 2). The direction of the shift depends on the orientation of the applied field (Fig. 3), indicating the presence of anisotropy in the ordered phase. For the simple easy-axis antiferromagnet [15,16], the resonance frequency is $f = \sqrt{(\gamma H)^2 \pm \Delta^2}$ (here γ is a gyromagnetic ratio, and Δ is a gap in the magnon spectrum) for the field applied perpendicular to the easy axis and along the easy axis above the spin-flop field, respectively. Thus, the observed increase in the resonance field for $\mathbf{H}||b$ confirms earlier identification of this axis as the easy axis of anisotropy [9].

To compare resonance field shifts $H(T)$ for different field orientations and different microwave frequencies we have calculated the apparent gap:

$$\Delta(T) = \sqrt{|f^2 - (\gamma H)^2|} = \gamma\sqrt{|H_{pm}^2 - H^2|}, \qquad (1)$$

where $H_{pm} = f/\gamma$ is the paramagnetic resonance field above the Néel temperature. The shift of the resonance field below

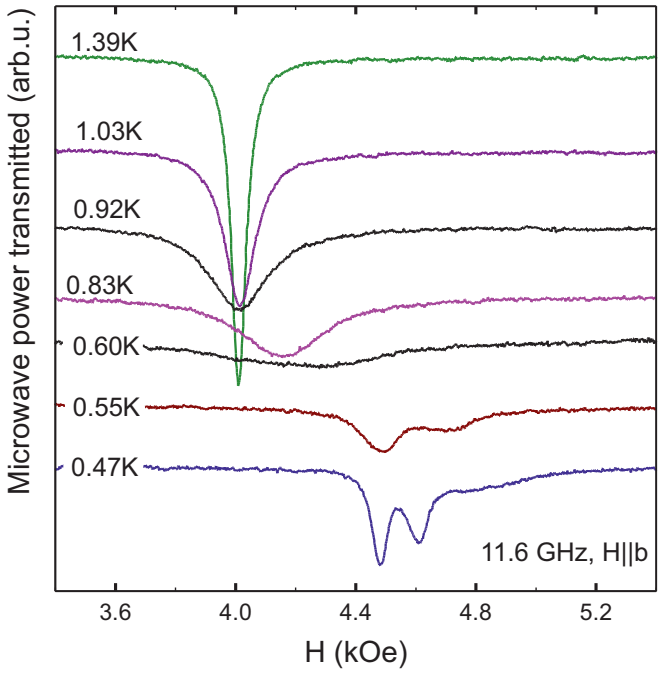

FIG. 2. Temperature evolution of the resonance absorption in $Cu(en)(H_2O)_2SO_4$ at low temperatures. $f = 11.6$ GHz, $\mathbf{H}||b$.

the transition temperature is smooth (see Fig. 3), which indicates continuous development of the order parameter and confirms the second-order phase transition. The apparent gap temperature dependence differs for $\mathbf{H}||a$ and $\mathbf{H}||c^*$, which indicates that anisotropy is biaxial. The transition temperature

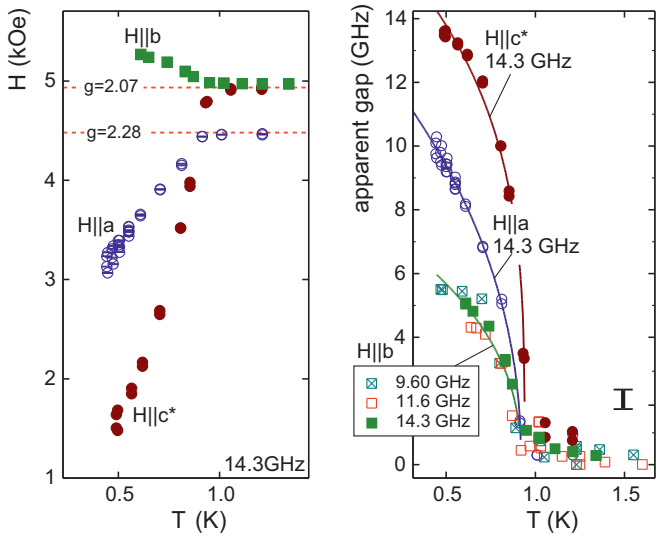

FIG. 3. Left: Temperature dependencies of the resonance field for three principal field directions, $f = 14.3$ GHz. Horizontal dashed lines mark the paramagnetic resonance field for the g factor values for corresponding field directions. Right: Temperature dependencies of the apparent gap for three principal field directions. Symbols show the experimental data; solid lines show phenomenological fits of the temperature behavior of the gap below the transition point as described in the text. The vertical bar shows the error estimate.

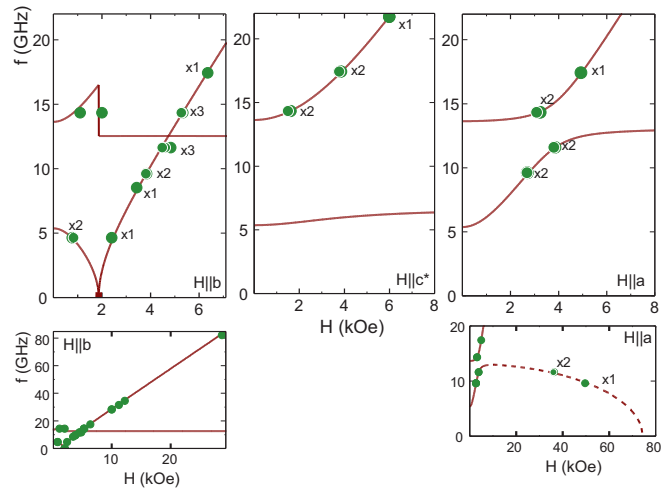

FIG. 4. Frequency-field diagrams of resonance absorption at the base temperature $T = 0.45$ K. The top row shows low-frequency and low-field parts of $f(H)$; the bottom row shows higher-frequency or higher-field $f(H)$ for principal field directions. Symbols show experimental data, solid lines show low-field theory as described in the text, and the dashed line shows the high-field fit as described in the text. Numbers at data points x1, x2, and x3 show the number of split components observed below 0.6 K at a particular frequency.

determined from the ESR experiment is $T_N = (0.92 \pm 0.02)$ K; it is in agreement with the known results.

For $\mathbf{H}||a, c^*$ (perpendicular to the easy axis) the apparent gap is proportional to the order parameter [16]. To quantify the determined order parameter temperature dependence we fitted $\Delta(T)$ data by the phenomenological law $\Delta \propto (1 - T/T_N)^{\beta}$ in the full temperature range from the base temperature of 0.45 K to T_N; the phenomenological exponent values are 0.40 ± 0.02 and 0.31 ± 0.03 for $\mathbf{H}||a, c^*$, respectively. The obtained exponent values are close to the critical exponent values for the 3D Ising model $\beta_{\text{Ising}}^{(3D)} \approx 0.327$ [17], 3D XY-model $\beta_{XY}^{(3D)} = 0.3485$ [18], and 3D Heisenberg model $\beta \approx 0.36$ [19]. All three models could be relevant for CUEN at various fields and temperatures: magnetization studies at 0.5 K [9] revealed the effect of intrinsic spin anisotropies for all field orientations at $H < 2$ kOe, which corresponds to the Ising model; at higher fields the potential prevalence of the field-induced easy-plane anisotropy can be expected, resulting in the preference of the XY model at the lowest temperatures, while at some higher temperatures, a crossover to isotropic Heisenberg behavior occurs [12]. Similar interpretation of the $\Delta(T)$ dependence at $\mathbf{H}||b$ is not possible: within the mean-field model the position of the resonance absorption for the field applied along the easy axis depends not only on the magnon gap but also on the temperature-dependent longitudinal susceptibility [15], which has unusual temperature dependence in CUEN [9]. However, our data can be reasonably fitted by the phenomenological law with $\beta = 0.50 \pm 0.07$.

We have collected the resonance absorption curves at the base temperature of 0.45 K for different frequencies for $\mathbf{H}||a, b, c^*$. The final frequency-field diagrams are shown in Fig. 4. The observed $f(H)$ dependencies are in qualitative agreement with the known case of a two-sublattice antiferromagnet with two axes of anisotropy [15].

Besides the monotonous shift of the resonance absorption below T_N, development of a certain "fine structure" of the resonance line was observed on cooling below approximately 0.6 K (Fig. 2). This splitting of the resonance line was observed in all three field orientations studied; its magnitude is up to 100–150 Oe and is much smaller than the resonance field value. The possible origin of this splitting will be discussed in the following sections; note, however, that the standard model of antiferromagnetic resonance in a collinear antiferromagnet does not allow such a splitting.

IV. DISCUSSION

A. Frequency-field diagram analysis

Magnetic resonance spectroscopy is a sensitive and informative method to study antiferromagnetic ordering. At the transition point the single-mode paramagnetic resonance absorption spectrum transforms into a multimode antiferromagnetic resonance (AFMR) absorption spectrum with nonlinear $f(H)$ dependence. For a collinear antiferromagnet there are always only two low-energy modes [15,16,20], while for a noncollinear antiferromagnet there should be three low-energy modes [20] with completely different $f(H)$ diagrams (see, e.g., [21–28]). We observe (save for the small splitting of resonance lines which will be addressed later) only two modes of antiferromagnetic resonance (Fig. 4) with $f(H)$ dependencies typical of a collinear antiferromagnet. Thus, we can definitely conclude that the antiferromagnetic ordering in $Cu(en)(H_2O)_2SO_4$ is collinear.

Softening of one of the resonance modes in $\mathbf{H}||b$ at approximately 2 kOe marks a spin-flop transition observed previously in a low-temperature magnetization study [9]; this observation proves that the b axis is the easy axis of anisotropy.

Distinct $f(H)$ and $\Delta(T)$ dependencies for $\mathbf{H}||a, c^*$ (Figs. 3 and 4) indicate that the anisotropy is biaxial. The $f(H)$ dependencies for the biaxial collinear antiferromagnet (see, e.g., Ref. [15]) are characterized by two zero-field gaps $\Delta_1 > \Delta_2$. Identification of the anisotropy axes from the AFMR data is model independent: For the field applied exactly along the hard or second-easy axis one of the eigenmodes is field independent. The field-dependent AFMR mode corresponds to the oscillations of the order parameter from its equilibrium position along the easy axis toward the field direction and back [15,16]. Since the energy cost is smaller for the deviations toward the second-easy axis, the field-dependent mode starts from the lower gap Δ_2 for the field applied along the second-easy axis (close to $\mathbf{H}||a$ in our case). Consequently, the hard axis of anisotropy (the less favorable orientation of the order parameter) is close to the c^* axis.

Quantitative analysis of the AFMR $f(H)$ curves was performed within the hydrodynamic approach framework [20]. This approach is valid well below the saturation field; this condition is fulfilled for most of our data ($H_{sat} \approx 70$ kOe for CUEN). Low-energy spin dynamics of the collinear antiferromagnet at $T = 0$ is described as the uniform oscillations of the order parameter vector field with the Lagrangian density:

$$\mathcal{L} = \frac{\chi_\perp}{2\gamma^2}(\dot{\mathbf{l}} + \gamma[\mathbf{l} \times \mathbf{H}])^2 - U_A, \tag{2}$$

where unit vector $\mathbf{l}$ is the collinear AFM order parameter (which is the normed vector of the staggered magnetization for the sublattices model), γ is the gyromagnetic ratio, $\chi_\perp$ is the transverse susceptibility, and $U_A(\mathbf{l})$ is the anisotropy energy depending on the order parameter orientation:

$$U_A = \frac{a_1}{2} l_X^2 + \frac{a_2}{2} l_Y^2 + \xi \chi_\perp (\mathbf{lH}) l_a H_a, \tag{3}$$

where the first two terms describe conventional biaxial anisotropy, $a_1 > a_2 > 0$, with X and Y being the directions of the hard (X) and second easy (Y) axes, and the last term describes axial g factor anisotropy (within the mean-field approach $\xi = \Delta g/g$ [29]) with the g-tensor principal axis coinciding with the a axis [14]. Due to the low symmetry of $Cu(en)(H_2O)_2SO_4$ only one axis (easy axis Z) is pinned to the only second-order crystallographic axis b, while the orientation of the hard and second easy axes in the (ac) plane is arbitrary. A detailed model description is given in the Appendix.

This model was then used to fit the $f(H)$ data for all orientations simultaneously using the least-squares method. The GNU OCTAVE [30] software, with its standard minimization routines, was used for the fitting procedure; the OCTAVE script used for the AFMR frequencies calculations is available in Ref. [31]. The resulting best fit is shown in Fig. 4 as a solid line. It well describes our experimental data; the best fit parameters are the gaps $\Delta_1 = \gamma\sqrt{a_1/\chi_\perp} = (13.6 \pm 0.1)$ GHz and $\Delta_2 = \gamma\sqrt{a_2/\chi_\perp} = (5.37 \pm 0.05)$ GHz, the gyromagnetic ratio $\gamma = (2.88 \pm 0.01)$ GHz/kOe (corresponding to $g = 2.06$), the g factor anisotropy parameter $\xi = (0.10 \pm 0.02)$, and the angle between the hard axis and the c^* axis $|\phi| = (18 \pm 2)^\circ$. We cannot determine the direction of rotation from the hard axis toward the c^* axis (clockwise or counterclockwise) from our data. The value of Δ_2 is close to the value of 0.3 K (6.3 GHz) predicted in Ref. [9] from the analysis of low-temperature magnetization curves.

Besides the low-field resonance absorption, we observed a high-field absorption signal at $\mathbf{H}||a$ (Fig. 4). Taking into account that for $\mathbf{H}||a$ the field is applied at the angle ϕ from the second easy axis, we fit the $f(H)$ dependence for the softening mode as (see Appendix)

$$f = \Delta_{\text{eff}}\sqrt{1 - (H/H_{\text{sat}})^2}, \tag{4}$$

where $\Delta_{\text{eff}}(\phi) = \sqrt{\Delta_1^2 \sin^2\phi + \Delta_2^2 \cos^2\phi}$ ($\Delta_{\text{eff}} = 13.1$ GHz for the $\mathbf{H}||a$ experiment).

The best-fit value for the saturation field $H_{\text{sat}} = (74 \pm 1)$ kOe is slightly larger than the value of 63 kOe determined from the phase diagram of Refs. [9,12]. This overestimation of the saturation field is quite natural for the quasi-low-dimensional magnet. The mean-field sublattice model [16] assumes a linear magnetization process up to the saturation field with the maximal magnetization $M_0 = \chi_\perp H_{\text{sat}}$. The magnetization process of low-dimensional magnets is nonlinear with positive curvature at high fields [1], as observed for CUEN as well [9]; hence, the real saturation field is less than $M_0/\chi_\perp$.

B. Microscopic contributions to the anisotropy of the ordered phase and interplane ordering pattern

Experimental identification of the anisotropy axes differs from the predictions of Refs. [9,14]. We will discuss below possible microscopic contributions to the anisotropy of the antiferromagnetically ordered state of $Cu(en)(H_2O)_2SO_4$ and will demonstrate that accurate accounting for dipolar coupling explains this controversy and allows us to determine the interplane ordering pattern.

Within the mean-field approach the AFMR gaps are $\Delta_{1,2} = \gamma\sqrt{2H_{A1,A2}H_E}$, where $H_E = H_{\rm sat}/2$ and $H_{A1,A2}$ represent exchange and anisotropy fields [16,32]. The effective fields for CUEN are $H_E = 32$ kOe, $H_{A1} = 0.35$ kOe, and $H_{A2} = 0.054$ kOe. While the effective fields are determined with approximately 20% uncertainty, keeping in mind the aforementioned nonlinearity of the magnetization process of two-dimensional CUEN [9], the ratio $H_{A1}/H_{A2} = (\Delta_1/\Delta_2)^2 = 6.41 \pm 0.07$ is determined much more reliably since it does not depend on the exact exchange field value.

Three possible contributions to the anisotropy of the ordered phase can be considered: dipole-dipole interaction, symmetric anisotropic spin-spin coupling (anisotropic exchange interaction), and Dzyaloshinskii-Moria coupling. The symmetric anisotropic interaction was analyzed in Refs. [9,14] as the possible source of the anisotropy of static magnetization and of the anisotropic ESR resonance field shift. Since both g-tensor anisotropy and the symmetric anisotropic coupling originate from the same spin-orbit coupling, one can conclude [9,15] that the symmetric anisotropic coupling favors easy-plane anisotropy with the main axis of the g tensor (a axis) being the hard axis. The estimate of the anisotropic symmetric coupling constant $\langle G\rangle \simeq 0.02$ K [14] corresponds to the effective anisotropy field $H_A \simeq \langle G\rangle/(2\mu_B) \simeq 0.15$ kOe (taking into account only four in-plane neighbors).

Estimates in Ref. [14] indicated that nearest-neighbor dipolar coupling could provide a remarkable contribution to this total anisotropy. To verify this conjecture, first, we calculated the dipolar contribution to the anisotropy energy of the coupled magnetic layers with intraplane collinear antiferromagnetic order. The strength of the dipolar coupling for nearest neighbors can be estimated as $\mu_B^2/(k_B d_{\rm min}^3) \simeq 4.3$ mK (0.063 kOe in terms of effective field); here $d_{\rm min} = 5.27$Å is the shortest Cu-Cu distance for CUEN. We consider two possible patterns of magnetic (bc) layer stacking: antiferromagnetic and ferromagnetic stacking of adjacent magnetic planes (Fig. 1). Here the terms ferro- and antiferromagnetic describe the change in the ion magnetization on the elementary translation $\mathbf{T} = (\mathbf{a} + \mathbf{b})/2$. Dipolar energy was calculated as a function of the order parameter orientation assuming fully saturated magnetization per ion and taking into account known uniaxial g factor anisotropy [14]. Neighbors at a distance up to 100 Å from the given ion were included in the dipolar sum. A further increase in the cutoff distance to 150 Å did not change the result. Results are shown in Fig. 5.

Clearly, the ferromagnetic ordering pattern reproduces well the observed anisotropy: The b axis with the minimum dipolar energy is the easy axis, the second-easy axis is within 10° of the a axis, and the hard axis is close to the c and c^* axes.

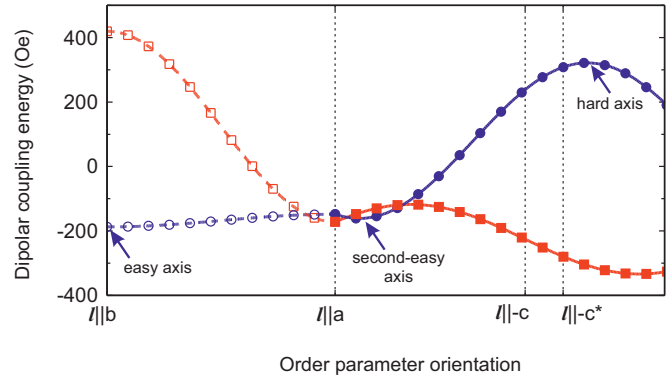

FIG. 5. Dependence of the dipolar coupling energy per spin (in terms of effective field) on the order parameter orientation for ferromagnetic (blue circles) and antiferromagnetic (red squares) stacking of adjacent (bc) planes. Symbols show computed values, and curves show the fit of the computed values by $A + B\cos[2(\varphi + \delta)]$; the shift δ is set to zero for the (ba)-plane rotation and is used as a fit parameter for the (ac)-plane rotation.

The anisotropy energy per spin is $U^{(\rm dip)} = U_0 + \mu H_{A1}^{(\rm dip)} l_X^2 + \mu H_{A2}^{(\rm dip)} l_Y^2$ (here μ is the magnetization per ion, X and Y are the hard and second easy axes, and $H_{A1}^{(\rm dip)} > H_{A2}^{(\rm dip)} > 0$), with $H_{A1}^{(\rm dip)} = 0.51$ kOe, $H_{A2}^{(\rm dip)} = 0.027$ kOe. The obtained ratio $H_{A1}^{(\rm dip)}/H_{A2}^{(\rm dip)} \approx 19$ is almost threefold higher than the experimentally measured value; therefore, the dipolar coupling alone cannot fully describe the observed anisotropy.

Interplane exchange couplings calculated from first principles [11] prefer the antiferromagnetic interplane stacking: the mean-field energy of the antiferromagnetic stacking pattern is 5.6 μeV per spin less (0.96 kOe in terms of the effective field). However, the dipolar contribution to the anisotropy for the antiferromagnetic stacking pattern completely disagrees with the experiment: The b axis would be the hard axis (Fig. 5).

From the above estimates one can see that the dipolar coupling and interplane exchange couplings could be competing in CUEN. In particular, above the spin-flop transition the order parameter is confined to the (ac) plane, and the dipolar energy is minimized for the antiferromagnetic interplane stacking (Fig. 5). This could result in the rearrangement of the interplane stacking pattern above the spin-flop transition

Next, we consider interplane Dzyaloshinskii-Moriya couplings. ESR linewidth analysis at high temperatures [14,33] demonstrated that only about a quarter of the total high-temperature linewidth is due to dipole-dipole couplings (calculated explicitly for CUEN [33]), while the remaining 75% of the linewidth is more likely due to interplane DM coupling. The combination of inversion centers and rotational axes creates a particular pattern of DM vectors which cancels out effects of DM interaction within the mean-field model. Inversion symmetry forbids DM coupling on all bonds except for the J_1 and J_2 bonds (Fig. 1). The J_1 bond couples ions within the (ab) plane. Two neighboring (ab) planes (these planes contain the ions marked as A, B1, and B2 and α, $\beta 1$, and $\beta 2$, respectively, in Fig. 1) are linked by the inversion, which makes DM vector patterns within these planes exactly opposite: $\mathbf{D}_{AB1} = -\mathbf{D}_{\alpha\beta 1}$, $\mathbf{D}_{AB2} = -\mathbf{D}_{\alpha\beta 2}$. Within the same

(ab)-plane projection of the DM vector on the second-order axis b alternates: $\mathbf{D}_{AB1} = (D_X, D_Y, D_Z)$, $\mathbf{D}_{AB2} = (D_X, D_Y, -D_Z)$, where we use the same XYZ basis, with the Z axis along the b axis and X and Y axes within the (ac) plane. When summed over all bonds within the mean-field model, this pattern of DM vectors cancels out exactly and yields no additional anisotropy. The J_2 bond couples next-nearest layers ($x = 0$ and $x = 1$ layers in Fig. 1); due to inversion symmetry the DM vectors on bonds originating from the B1 and β1 ions are opposite, which, again, yields no additional anisotropy.

Now we can sum up the dipolar contribution and the contribution of the symmetric anisotropic coupling:

$$U = U_0 + \mu H_A^{(\mathrm{sym})} l_a^2 + \mu H_{A1}^{(\mathrm{dip})} l_X^2 + \mu H_{A2}^{(\mathrm{dip})} l_Y^2, \qquad (5)$$

where l_a is the projection of the order parameter on the a axis and $H_A^{(\mathrm{sym})} > 0$. Neglecting the deviation of the second easy axis Y from the a axis, we found that $H_A^{(\mathrm{sym})} \approx (0.055 \pm 0.002)$ kOe reproduces the experimentally determined ratio of the resulting anisotropy fields. We can estimate the anisotropic symmetric coupling constant $zS^2G = \mu H_A^{\mathrm{sym}}$, where $z = 4$ is the number of seemingly equally contributing in-plane neighbors and $S = 1/2$. This estimate corresponds to $G \simeq 3.7$ mK, which is in reasonable agreement with the conventional estimate of the symmetric anisotropic coupling constant as $(\Delta g/g)^2 J$. The total anisotropy fields are then 0.51 and 0.08 kOe; these values are 30% larger than the values directly estimated from the AFMR experiment ($H_{A1} = 0.35$ kOe and $H_{A2} = 0.054$ kOe). This scaling can be partially due to the uncertainties in the exchange field definition.

Thus, we can conclude that the dipolar interaction plays the dominant role in the determination of the anisotropy in the ordered phase of $Cu(en)(H_2O)_2SO_4$ and that the AFMR data can be interpreted in favor of ferromagnetic ordering of the nearest planes.

C. AFMR line splitting

Observed splitting of the AFMR absorption line below approximately 0.6 K is not expected for the collinear antiferromagnet. Splitting magnitudes are listed in Table I and are shown in Fig. 6; the maximal splitting amplitude is about 100–150 Oe. The largest splitting is observed at the frequencies close to the magnon gaps. Whatever the splitting mechanism is, the later observation is quite natural: The slope of the AFMR frequency-field dependence df/dH approaches zero close to the magnon gaps; thus, the small variation of the resonance frequency could result in a substantial change of the resonance field. Several splitting mechanisms can be considered which could be responsible for the aforementioned splitting.

First, we have to consider the possibility of the sample twinning. To produce experimentally observed splitting values the sample should consist of a mosaic of crystallites rotated by $\sim 10^\circ$. However, the polarized light microscopy of our samples at room temperature does not show any presence of different blocks in the samples. The optical reflectometry at room temperature [34,35] does not reveal features that could be ascribed to sample twinning. The angular dependencies of the ESR absorption at $T > T_N$ measured at 9 GHz [14] and at 72 GHz (present work) also give no indication of the crystal twinning, while the small linewidth of the ESR absorption (10–20 Oe at 4.2 K) and g factor anisotropy would make 10° rotation of crystallites clearly apparent. Thus, sample twining as the source of the AFMR line splitting in CUEN can be ruled out decisively.

Another possibility arises from the quasi-two-dimensionality of $Cu(en)(H_2O)_2SO_4$. The two-dimensional Heisenberg antiferromagnet orders only at $T = 0$; however, the presence of Ising-type anisotropy results in ordering

TABLE I. Observed splitting of the AFMR line at different field orientations and microwave frequencies measured at a base temperature of 0.45 K

f (GHz)	average H_{res} (kOe)	ΔH (kOe)
	H$\|\|a$	
9.6	2.689	0.014 ± 0.005
11.6	3.824	0.041 ± 0.005
11.6	36.15	0.32 ± 0.04
14.3	3.157	0.13 ± 0.015
	H$\|\|b$	
4.64	0.75	0.059 ± 0.015
9.6	3.821	0.019 ± 0.005
11.6	4.546	0.123 ± 0.010
14.3	5.280	0.037 ± 0.007
14.3	5.280	0.053 ± 0.007
17.4	6.368	0.023 ± 0.008
31.6	11.194	0.021 ± 0.005
	H$\|\|c$	
14.3	1.560	0.16 ± 0.04
17.4	3.792	0.063 ± 0.015
21.7	5.912	0.051 ± 0.015

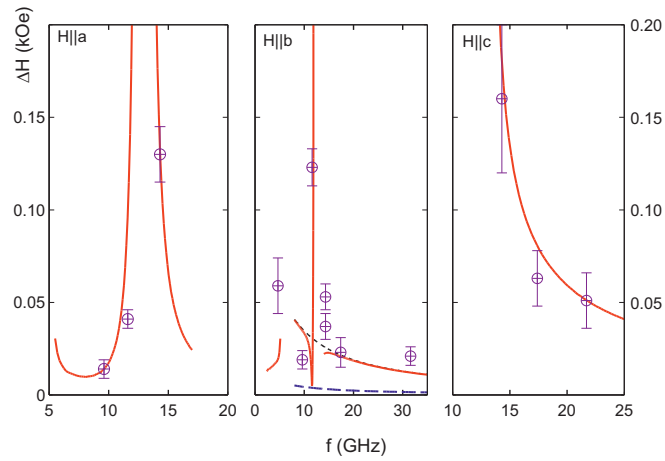

FIG. 6. Frequency dependence of the observed splitting of the AFMR resonance absorption line at the base temperature of 0.45 K (symbols). Solid curves show the model of two decoupled antiferromagnets with slightly different anisotropy parameters and the change in the anisotropy parameters above the spin-flop transition as described in the text. This model includes the 2° tilt of the magnetic field at the nominal **H**$\|\|b$ orientation. The dotted curve in the middle panel represents the same model assuming zero tilt at **H**$\|\|b$. The dashed curve corresponds to the model without a change in the anisotropy parameters above the spin-flop transition.

at finite temperature. Thus, in the extreme limit of very weak interplane coupling, the quasi-two-dimensional antiferromagnet can be considered a stack of equivalent antiferromagnetically ordered layers weakly coupled by interlayer Heisenberg exchange interactions. The eigenfrequencies of this system would split similarly to the known textbook problem of coupled oscillators. Such an effect was reported for another quasi-2D antiferromagnet, $RbFe(MoO_4)_2$ [36,37]. For the case of field applied along the symmetry axis, split components of resonance absorption correspond to the in-phase and out-of-phase oscillations of the coupled layers. However, the out-of-phase oscillations of the order parameters correspond to the out-of-phase oscillations of the uniform magnetization of individual layers, which strongly decouples this oscillation mode from the uniform microwave field. At the same time, the experiment (Fig. 2) shows that the split components have approximately the same integral intensity. This means that corresponding resonance modes are comparably coupled to the microwave field, which rules out the Heisenberg interlayer coupling as the source of the observed splitting.

Finally, we tried a semiphenomenological model assuming that below T_N two practically decoupled antiferromagnetic systems are formed within the $Cu(en)(H_2O)_2SO_4$ lattice. We can recall here the known case of formation of completely different ordering patterns in the neighboring layers of another quasi-two-dimensional antiferromagnet, $KFe(MoO_4)_2$, with independent spin dynamics of these layers [38,39]. We will describe these antiferromagnetic subsystems in CUEN phenomenologically by anisotropy parameters $a_{1,2}$ slightly different from those in Eq. (3):

$$a_{1,2}^{(\pm)} = a_{1,2}(1 \pm \delta_{1,2}). \tag{6}$$

The difference in AFMR resonance fields for two antiferromagnets with slightly different anisotropy constants was calculated numerically using best-fit values from Sec. IV A as starting parameters. We have found that $\delta_1 \neq \delta_2$ is required, and the satisfactory description of the data in Fig. 6 is achieved for $\delta_1 = 0.012$ and $\delta_2 = 0.005$.

However, this parameter set fails completely to describe splitting at the $\mathbf{H}||b$ orientation above the spin-flop transition (see the dashed line in Fig. 6). This can be fixed by assuming that the system-to-system variation of the small anisotropy constant a_2 increases almost tenfold in the fields exceeding the spin-flop transition field H_{SF} and can be described now by $\delta_2^{(H>H_{SF})} = 0.04$. The increase of the splitting close to the second magnon gap can be accounted for by a 2° tilt of the magnetic field, which is plausible for our experimental setup. The change in the effective anisotropy parameter after the spin-flop transition was previously reported for the square-lattice antiferromagnet $Cu(pz)_2(ClO_4)_2$ [40] and discussed as a possible effect of dipolar forces [41]. We recall here the possibility discussed in the previous section that the interplane ordering pattern is rearranged above the spin-flop transition due to the difference in dipolar coupling energy; such a rearrangement will surely result in the change in anisotropy constants.

From our results we cannot reliably conjecture about the origin of the possible formation of two decoupled slightly inequivalent magnetic systems at low temperature. One possible reason is a weak alternation of the crystal structure due to the magnetoelastic coupling leading to the inequivalence of odd and even layers. Verification of this hypothesis requires either a high-resolution structural analysis or a low-temperature NMR experiment to check the number of inequivalent copper ions in the antiferromagnetically ordered $Cu(en)(H_2O)_2SO_4$.

D. Spin dynamics above the Néel point

The phase diagram of $Cu(en)(H_2O)_2SO_4$ was previously discussed in the context of the field-induced BKT transition [9,12]. The applied magnetic field effectively creates an XY anisotropy as the short-range antiferromagnetic correlations develop at $T < \Theta_{CW}$. This field-induced anisotropy competes with thermal effects. In the case of CUEN a crossover from the Heisenberg to XY regime takes place below T_N for fields lower than 10 kOe, while for higher fields the crossover temperature rises, reaching 1.5 K at 20 kOe [12].

A 2D magnet with XY anisotropy undergoes a BKT transition; free vortex dynamics above the BKT transition temperature can affect the ESR linewidth, leading to characteristic exponential temperature dependence [42]. Thus, one could expect that the ESR linewidth temperature dependence in CUEN would change from critical behavior at low fields (below 10 kOe) to some combination of critical and XY behavior at higher fields, while pure XY behavior in a sufficiently large temperature interval above T_N could be expected above 40 kOe. However, to distinguish these regimes the ESR linewidths have to be measured very accurately, and even then, both scenarios are found to describe experimental data qualitatively well, and the preferable scenario can be chosen only after quantitative comparison of model parameters with the theoretical predictions [42].

To check for these effects we have measured ESR absorption above the Néel temperature at different microwave frequencies corresponding to resonance field values from 3 to 40 kOe; the latter value is about 2/3 of the saturation field. Accurate determination of ESR linewidth is handicapped in our experimental setup by the inhomogeneity of the magnetic field from a compact cryomagnet and distortions of the ESR line shape at high frequencies. We observed ESR linewidth of 20–30 Oe at 1.7 K, which broadens up to approximately 200 Oe at T_N. We did not observe a strong qualitative difference in temperature evolution of the ESR linewidth at different resonance fields, which can be interpreted as switching on the additional (vortex) channel of spin relaxation in the field-induced XY regime.

V. CONCLUSIONS

We have performed a detailed low-temperature ESR study of the quasi-2D antiferromagnet $Cu(en)(H_2O)_2SO_4$. Our results confirm that transition to the magnetically ordered state at 0.9 K is continuous; the ordered phase is a collinear antiferromagnetic state with the easy axis aligned along the crystallographic b axis and the second easy axis aligned in the (ac) plane at approximately 18° from the a axis. The observed anisotropy of the ordered phase can be largely described by dipolar coupling of copper spins; on the basis of this analysis

the ferromagnetic ordering pattern of the two-dimensional planes is favored.

We have observed additional splitting of the antiferromagnetic resonance absorption spectra, which can be interpreted as the coexistence of the two ordered antiferromagnets with slightly different anisotropy parameters. The microscopic origin of formation of these antiferromagnetic systems is unclear, and additional high-resolution structural or NMR experiments are required to get insight into the equivalence or inequivalence of two-dimensional magnetic subsystems of CUEN and the formed interplane ordering patterns.

ACKNOWLEDGMENTS

The authors thank Prof. A. I. Smirnov and Prof. L. E. Svistov (Kapitza Institute) for fruitful discussions and supporting comments. V.N.G. and Yu.V.K. acknowledge support of their experimental studies by Russian Science Foundation Grant No.17-02-01505 (experiments above 9 GHz) and Russian Foundation for Basic Research Grant No. 19-02-00194 (experiments below 9 GHz); data processing and modeling were supported by the program of fundamental studies of HSE. Work at P. J. Šafárik University (R.T. and A.O.) was supported by Scientific Grant Agency of the Ministry of Education, Science, Research and Sport of the Slovak Republic, VEGA Grant 1/0269/17. J.C. acknowledges support of his work by Path to Exascale Project No. CZ.02.1.01/0.0/0.0/16-013/0001791 and by Ministry of Education, Youth and Sports of Czech Republic, National Program of Sustainability II, Project No. LQ1605.

APPENDIX: EQUATIONS FOR ANTIFERROMAGNETIC RESONANCE FREQUENCIES

We use the macroscopic (hydrodynamic) approach of Ref. [20]. For the collinear antiferromagnet Lagrangian density is

$$\mathcal{L} = \frac{\chi_\perp}{2\gamma^2}(\dot{\mathbf{l}} + \gamma[\mathbf{l}\times\mathbf{H}])^2 - U_A, \tag{A1}$$

where $\mathbf{l}$ is the collinear antiferromagnetic order parameter, γ is the gyromagnetic ratio, and U_A is the anisotropy energy. In the case of the monoclinic crystal with the easy axis Z locked onto the only second-order axis, the anisotropy energy can be written as

$$U_A = \frac{a_1}{2}l_X^2 + \frac{a_2}{2}l_Y^2, \tag{A2}$$

where $a_1 > a_2 > 0$ and X and Y are the directions of the hard and second easy axes, respectively.

The uniaxial g factor anisotropy (following Ref. [14]) can be included in the anisotropy energy [29]:

$$U_{A,g} = \xi\chi_\perp(\mathbf{l}\cdot\mathbf{H})l_a H_a; \tag{A3}$$

within the mean-field model $\xi = \Delta g/g$, l_a and H_a are the projections of the order parameter and magnetic field on the g-tensor principal axis [which is the a axis for $Cu(en)(H_2O)_2SO_4$]. For $\mathbf{H}||a$ this term results in the scaling of the gyromagnetic constant to $\gamma_{\rm eff}^2 = \gamma^2(1+2\xi)$.

Eigenfrequencies of the order parameter oscillation can be found from the linearized Euler-Lagrange equations. This yields two zero-field magnon gaps, $\Delta_{1,2} = \gamma\sqrt{a_{1,2}/\chi_\perp}$, $\Delta_1 > \Delta_2$. At $\mathbf{H}||b$ the spin-flop transition takes place at $H_{SF} = \Delta_2/\gamma$.

The resonance frequencies for $\mathbf{H}||b$ are

$$f_{1,2}^2 = \gamma^2H^2 + \frac{\Delta_1^2+\Delta_2^2}{2} \pm\sqrt{2\left(\Delta_1^2+\Delta_2^2\right)\gamma^2H^2 + \frac{\Delta_1^2-\Delta_2^2}{4}} \tag{A4}$$

for $H < H_{SF}$ and

$$f_1^2 = \Delta_1^2 - \Delta_2^2, \quad f_2^2 = \gamma^2H^2 - \Delta_2^2 \tag{A5}$$

for $H > H_{SF}$.

For $\mathbf{H}\perp b$ ($\mathbf{H}||a, c^*$) the secular equation is

$$\begin{vmatrix} \gamma_{\rm eff}^2H_XH_Y & -f^2+\Delta_2^2+\gamma_{\rm eff}^2H_Y^2 \\ f^2-\Delta_1^2-\gamma_{\rm eff}^2H_X^2 & -\gamma_{\rm eff}^2H_XH_Y \end{vmatrix} = 0, \tag{A6}$$

where $\gamma_{\rm eff} = \gamma$ for $\mathbf{H}||c^*$ and $\gamma_{\rm eff} = \gamma\sqrt{1+2\xi}$ for $\mathbf{H}||a$.

At high fields one of the AFMR modes asymptotically approaches Larmor frequency γH, and the frequency of the other AFMR mode remains small (it does not exceed the larger gap Δ_1) and softens at the saturation field [16]. While the hydrodynamical approach is not directly applicable at high fields, it can be shown that at high fields the angular dependence of the low-frequency AFMR mode resonance frequency is a universal function for a given antiferromagnet [43]. Thus, we can calculate the asymptotic frequency of the low-frequency mode within the low-field hydrodynamic approach for the field $\mathbf{H}\perp Z$:

$$\Delta_{\rm eff}(\phi) = \sqrt{\Delta_1^2\sin^2\phi + \Delta_2^2\cos^2\phi}, \tag{A7}$$

where the angle ϕ is counted from the hard axis. Combining Eq. (A7) with the predictions of the sublattices model [16], one obtains the resonance frequency of the low-frequency AFMR mode:

$$f = \Delta_{\rm eff}\sqrt{1-(H/H_{\rm sat})^2}. \tag{A8}$$

[1] L. J. de Jongh and A. R. Miedema, Experiments on simple magnetic model systems, Adv. Phys. **23**, 1 (1974) [reprinted in **50**, 947 (2010)].

[2] V. Zapf, M. Jaime, and C. D. Batista, Bose-Einstein condensation in quantum magnets, Rev. Mod. Phys. **86**, 563 (2014).

[3] N. A. Fortune, S. T. Hannahs, Y. Yoshida, T. E. Sherline, T. Ono, H. Tanaka, and Y. Takano, Cascade of Magnetic-Field-Induced Quantum Phase Transitions in a Spin-1/2 Triangular-Lattice Antiferromagnet, Phys. Rev. Lett. **102**, 257201 (2009).

[4] M. E. Zhitomirsky and H. Tsunetsugu, Magnon pairing in quantum spin nematic, Europhys. Lett. **92**, 37001 (2010).

[5] O. A. Starykh, Unusual ordered phases of highly frustrated magnets: A review, Rep. Prog. Phys. **78**, 052502 (2015).

[6] A. Cuccoli, T. Roscilde, R. Vaia, and P. Verrucchi, Field-induced XY behavior in the $S = 1/2$ antiferromagnet on the square lattice, Phys. Rev. B **68**, 060402(R) (2003).

[7] A. Cuccoli, T. Roscilde, R. Vaia, and P. Verrucchi, Detection of XY Behavior in Weakly Anisotropic Quantum Antiferromagnets on the Square Lattice, Phys. Rev. Lett. **90**, 167205 (2003).

[8] J. V. José, *40 Years of BKT Theory* (World Scientific, London, 2013).

[9] L. Lederová, A. Orendáčová, J. Chovan, J. Strečka, T. Verkholyak, R. Tarasenko, D. Legut, R. Sýkora, E. Čižmár, V. Tkáč, M. Orendáč, and A. Feher, Realization of a spin-1/2 spatially anisotropic square lattice in a quasi-two-dimensional quantum antiferromagnet $Cu(en)(H_2O)_2SO_4$, Phys. Rev. B **95**, 054436 (2017).

[10] M. Kajňaková, M. Orendáč, A. Orendačová, A. Vlček, J. Černák, O. V. Kravchyna, A. G. Anders, M. Bałanda, J.-H. Park, A. Feher, and M. W. Meisel, $Cu(H_2O)_2(C_2H_8N_2)SO_4$: A quasi-two-dimensional $S = 1/2$ Heisenberg antiferromagnet, Phys. Rev. B **71**, 014435 (2005).

[11] R. Sýkora and D. Legut, Magnetic interactions in a quasi-one-dimensional antiferromagnet $Cu(H_2O)_2(en)SO_4$, J. Appl. Phys. **115**, 17B305 (2014).

[12] L. Baranová, A. Orendáčová, E. Čižmar, R. Tarasenko, V. Tkáč, M. Orendáč, and A. Feher, Fingerprints of field-induced Berezinskii-Kosterlitz-Thouless transition in quasi-two-dimensional S=1/2 Heisenberg magnets $Cu(en)(H_2O)_2SO_4$ and $Cu(tn)Cl_2$, J. Magn. Magn. Mater. **404**, 53 (2016).

[13] P. Sengupta, C. D. Batista, R. D. McDonald, S. Cox, J. Singleton, L. Huang, T. P. Papageorgiou, O. Ignatchik, T. Herrmannsdorfer, J. L. Manson, J. A. Schlueter, K. A. Funk, and J. Wosnitza, Nonmonotonic field dependency of the Neel temperature in the quasi-two-dimensional magnet $[Cu(HF_2)(pyz)_2]BF_4$, Phys. Rev. B **79**, 060409(R) (2009).

[14] R. Tarasenko, A. Orendáčová, E. Čižmár, S. Matas, M. Orendáč, I. Potocnak, K. Siemensmeyer, S. Zvyagin, J. Wosnitza, and A. Feher, Spin anisotropy in $Cu(en)(H_2O)_2SO_4$: A quasi-two-dimensional $S = 1/2$ spatially anisotropic triangular-lattice antiferromagnet, Phys. Rev. B **87**, 174401 (2013).

[15] T. Nagamiya, K. Yosida, and R. Kubo, Antiferromagnetism, Adv. Phys. **4**, 1 (1955).

[16] A. G. Gurevich and G. A. Melkov, *Magnetization Oscillations and Waves* (CRC Press, Boca Raton, FL, 1996).

[17] M. Kolesik and M. Suzuki, Accurate estimates of 3D Ising critical exponents using the coherent-anomaly method, Phys. A (Amsterdam, Neth.) **215**, 138 (1995).

[18] M. Campostrini, M. Hasenbusch, A. Pelissetto, P. Rossi, and E. Vicari, Critical behavior of the three-dimensional XY universality class, Phys. Rev. B **63**, 214503 (2001).

[19] C. Holm and W. Janke, Critical exponents of the classical three-dimensional Heisenberg model: A single-cluster Monte Carlo study, Phys. Rev. B **48**, 936 (1993).

[20] A. F. Andreev and V. I. Marchenko, Symmetry and the macroscopic dynamics of magnetic materials, Sov. Phys. Usp. **23**, 21 (1980).

[21] L. A. Prozorova, V. I. Marchenko, and Yu. V. Krasnyak, Magnetic resonance in the noncollinear antiferromagnet $Mn_3Al_2Ge_3O_{12}$, JETP Lett. **41**, 637 (1985).

[22] I. A. Zaliznyak, V. I. Marchenko, S. V. Petrov, L. A. Prozorova, and A. V. Chubukov, Magnetic resonance in the noncollinear antiferromagnet $CsNiCl_3$, JETP Lett. **47**, 211 (1988).

[23] L. E. Svistov, L. A. Prozorova, A. M. Farutin, A. A. Gippius, K. S. Okhotnikov, A. A. Bush, K. E. Kamentsev, and E. A. Tishchenko, Magnetic structure of the quasi-one-dimensional frustrated antiferromagnet $LiCu_2O_2$ with S=1/2, J. Exp. Theor. Phys. **108**, 1000 (2009).

[24] H. Tanaka, T. Ono, Sh. Maruyama, S. Teraoka, K. Nagata, H. Ohta, S. Okubo, Sh. Kimura, T. Kambe, H. Nojiri, and M. Motokawa, Electron Spin Resonance in Triangular Antiferromagnets, J. Phys. Soc. Jpn. **72**, 84 (2003).

[25] S. S. Sosin, L. A. Prozorova, P. Bonville, and M. E. Zhitomirsky, Magnetic excitations in the geometrically frustrated pyrochlore antiferromagnet $Gd_2Sn_2O_7$ studied by electron spin resonance, Phys. Rev. B **79**, 014419 (2009).

[26] S. S. Sosin, A. I. Smirnov, L. A. Prozorova, G. Balakrishnan, and M. E. Zhitomirsky, Magnetic resonance in the pyrochlore antiferromagnet $Gd_2Ti_2O_7$, Phys. Rev. B **73**, 212402 (2006).

[27] Yu. V. Krasnikova, V. N. Glazkov, and T. A. Soldatov, Experimental study of antiferromagnetic resonance in noncollinear antiferromagnet $Mn_3Al_2Ge_3O_{12}$, J. Exp. Theor. Phys. **125**, 476 (2017).

[28] V. Glazkov, T. Soldatov, and Yu. Krasnikova, Numeric calculation of antiferromagnetic resonance frequencies for the noncollinear antiferromagnet, Appl. Magn. Reson. **47**, 1069 (2016).

[29] V. N. Glazkov, A. I. Smirnov, A. Revcolevschi, and G. Dhalenne, Magnetic resonance study of the spin-reorientation transitions in the quasi-one-dimensional antiferromagnet $BaCu_2Si_2O_7$, Phys. Rev. B **72**, 104401 (2005).

[30] GNU OCTAVE, https://www.gnu.org/software/octave/.

[31] V. Glazkov, Numerical calculation of antiferromagnetic resonance frequencies for collinear antiferromagnets, http://www.kapitza.ras.ru/rgroups/esrgroup/numa.html.

[32] In the case of uniaxial anisotropy, the anisotropy energy per magnetic ion $U_A = Kl_z^2$ corresponds to the anisotropy field $H_A = K/\mu$, where μ is the magnetization of the ion.

[33] O. V. Kravchina, A. I. Kaplienko, E. P. Nikolova, A. G. Anders, D. V. Ziolkovskii, A. Orendáčová, and M. Kajnakova, Hydrogen bond and exchange interaction in the $(CuSO_4)(en) \cdot 2H_2O$ and $(CuSO_4)(en) \cdot 2D_2O$ organometallic compounds, Russ. J. Phys. Chem. B **5**, 2019 (2011).

[34] R. Sýkora, K. Postava, D. Legut, and R. Tarasenko, Optical properties of a monoclinic insulator $Cu(H_2O)_2(en)SO_4$, Acta Phys. Pol. A **127**, 469 (2015).

[35] R. Sýkora, K. Postava, D. Legut, and R. Tarasenko, Calculated reflection coefficients of a single planar interface with an optically biaxial $Cu(en)(H_2O)_2SO_4$ material compared to experiment, J. Nanosci. Nanotechnol. **16**, 7818 (2016).

[36] L. E. Svistov, A. I. Smirnov, L. A. Prozorova, O. A. Petrenko, L. N. Demianets, and A. Ya. Shapiro, Quasi-two-dimensional antiferromagnet on a triangular lattice $RbFe(MoO_4)_2$, Phys. Rev. B **67**, 094434 (2003).

[37] A. I. Smirnov, H. Yashiro, S. Kimura, M. Hagiwara, Y. Narumi, K. Kindo, A. Kikkawa, K. Katsumata, A. Ya. Shapiro, and L. N. Demianets, Triangular lattice antiferromagnet $RbFe(MoO_4)_2$ in high magnetic fields, Phys. Rev. B **75**, 134412 (2007).

[38] A. I. Smirnov, L. E. Svistov, L. A. Prozorova, A. Zheludev, M. D. Lumsden, E. Ressouche, O. A. Petrenko, K. Nishikawa, S. Kimura, M. Hagiwara, K. Kindo, A. Ya. Shapiro, and L. N. Demianets, Chiral and Collinear Ordering in a Distorted Triangular Antiferromagnet, Phys. Rev. Lett. **102**, 037202 (2009).

[39] L. E. Svistov, A. I. Smirnov, L. A. Prozorova, O. A. Petrenko, A. Ya. Shapiro, and L. N. Dem'yanets, On the possible coexistence of spiral and collinear structures in antiferromagnetic $KFe(MoO_4)_2$, JETP Lett. **80**, 204 (2004).

[40] K. Yu. Povarov, A. I. Smirnov, and C. P. Landee, Switching of anisotropy and phase diagram of the Heisenberg square-lattice $S = 1/2$ antiferromagnet $Cu(pz)_2(ClO_4)_2$, Phys. Rev. B **87**, 214402 (2013).

[41] A. V. Syromyatnikov, Spin-flop transition accompanied with changing the type of magnetic ordering, J. Magn. Magn. Mater. **426**, 279 (2017).

[42] M. Heinrich, H.-A. Krug von Nidda, A. Loidl, N. Rogado, and R. J. Cava, Potential Signature of a Kosterlitz-Thouless Transition in $BaNi_2V_2O_8$, Phys. Rev. Lett. **91**, 137601 (2003).

[43] A. M. Farutin and V. I. Marchenko, High-field low-frequency spin dynamics, JETP Lett. **83**, 238 (2006).